Comparison of low Reynolds number turbulence and conjugate heat transfer modelling for pin-fin roughness elements

Jens Bauer, James Tyacke[a*]

[a]*Brunel University London, Kingston Ln, Uxbridge UB8 3PH*

Abstract

This study contrasts Reynolds-Averaged Navier-Stokes (RANS) and (Numerical) Large-Eddy Simulation (NLES) for their use in predicting conjugate heat transfer for a low Reynolds number flow over surface roughness elements. The (N)LES predictions are in good agreement with experimental data, the heat transfer estimate being within 7.7% error. The linear RANS model shows larger errors up to 40%, especially in modelling the turbulent stresses. Using a one-equation LES turbulence model slightly improves the heat transfer prediction compared to a numerical LES. This indicates that more advanced turbulence models might not give significantly more accurate heat transfer predictions.

Additionally, this study investigates the time dependant development of the flow and temperature fields and how long data needs to be collected for statistically stationary results. The flow needs to develop for approximately 1800 through-flow times, T_L, and 150 T_L is required for collection of statistics. A significant range in turbulence length scale prediction between (N)LES and RANS was found. (N)LES scales appeared physically reasonable and should inform mesh resolution in future studies. Two additional cases were run with different cube heights showing changes in the time dependant development of the temperature field and greater sensitivity to turbulence modelling.

*Corresponding author, email address: james.tyacke@brunel.ac.uk

This research did not receive any specific grant from funding agencies in the public or commercial sectors. Computational resources at Brunel University London are gratefully acknowledged. Data presented can be accessed using the following DOI: 10.17633/rd.brunel.17068322.

Keywords: CFD, RANS, LES, Surface roughness, Electronics, Conjugate heat transfer

1. Introduction

The use of electronic systems is a cornerstone of modern life and electronic systems become more complex every year, with more components and advanced manufacturing methods. One of the major problems for electronics is the excess heat that is generated. The life span of an electronic device decreases exponentially with an increase in operating temperature [1], a 9 °C rise in operating temperature can half the service life of a component [2], therefore, temperature-dependent failures are the most common defect in electronic components and comprise 55% of all failure [3].

A surface roughness elements has the shape of electronic components, such as voltage regulators, memory chips, capacitors, and heat sinks. Heat removal from roughness elements is a key factor for the functionality of an electronic system. Areas of applications are square pinned heat sinks in desktops and laptops which are usually active air-cooled systems. In addition to this, data centres are predicted to use up to 20 % of the electricity produced in western countries by 2025 [4]. About 38 % of this energy is used to cool the electronics in large data centres and servers [5]. A similar trend is also seen in the automotive industry, as electric cars become more popular and the battery size keeps increasing, thermal management becomes more important. The power density in electric cars continues to increase and the fast charging of more than 100 kW leads to an increase in rejected heat that needs to be dissipated [6]. Thus, car batteries and electronic components need to be able to withstand continuous increases in power density and heat dissipation.

Aeroengine turbine blade cooling contains bluff body features of varying aspect which experience similar life degradation as electronic devices. Aeroengine

turbine blade cooling using roughness elements include internal cooling passage ribs, pin-fin arrays and trailing edge cutback pedestals [7], [8]. Moreover, the aerospace industry is currently developing more effective turbines and electric powered aeroplanes. Hybrid aircraft require a higher maximum onboard power and significantly increased supply voltage. The power density of the electrical components needs to be quadrupled [9] to 10-15 kW/kg by 2030 [10] which will lead to significantly more excess heat that needs to be dissipated via the electronics packaging. By creating more advanced and efficient cooling solutions, the efficiency and reliability of these systems can be increased. Computational fluid dynamics (CFD) is an important part of the design process because it provides deeper insight into the underlying flow features and heat transfer of roughness elements.

1.2 Computational fluid dynamics in heat transfer modelling.

Steady CFD is not always accurate in predicting the temperature of critical components. However, it is an important tool for estimating flow structures and improving designs for heat transfer optimization if trends can be identified reliably. The most used model in CFD is the Reynolds Averaged Navier–Stokes (RANS) with a linear turbulence models with wall functions, a historic overview and short description of different models is given by Rodi [11]. The significant problem with the linear turbulence models are that they assumes the eddy viscosity to be similar for all Reynolds stresses [12]. RANS solutions are highly dependent on the turbulence model and near-wall treatment, which provide different solutions depending on the chosen models. Dhinsa et al. (2005) [13] compare different turbulence models and their impact on the accuracy of the simulation. They found that, even for a very simple flow over a cube, the standard high Reynolds number k-ϵ model does not predict the flow structures accurately. All models used in the study demonstrate high errors in modelling the turbulence, while the hybrid k-ϵ/k-l model produces the best results.

Another study obtained the same results [14]. They determined that, for complex flow systems, the difference between the simulation and experimental re-

sults can be up to 20%. Steady-state RANS is not able to accurately model flow separation, recirculation, reattachment which are key for heat transfer. They do not deliver consistent and accurate heat transfer prediction. However, it is still a useful tool, especially due to its low computational cost [15],[16]. Other methods, such as unsteady RANS (URANS), hybrid RANS/LES, Detached Eddy Simulation (DES) or Large Eddy Simulation (LES) will deliver better results, but with an increased computational cost. URANS simulations over two square blocks [17] and twin impinging jets [18] show that the URANS simulation can offer better results than steady-state RANS. Karabelas el al. [19] use URANS to compute the flow around a still and rotating cylinder and compared their results to LES data. They showed that for averaged data, the k-ϵ RANS model results match the LES data for most of the domain. However, URANS is also not able to accurately resolve turbulent structures, and its theoretical basis is tenuous where there is a lack of separation between deterministic and dissipative scales. This is often found in low Reynolds number flows pertaining to electronics cooling. For further discussion about RANS turbulent modelling, please see [20].

Employing hybrid RANS/LES models clearly shows improved accuracy for the flow past a circular cylinder [21]. URANS is used near the wall and LES is employed in the rest of the flow. A hybrid URANS–Numerical-LES (RANS/NLES) model can predict the flow behaviour of a seal flow within 5% accuracy [22]. This is also the case for internal wall-bounded flows [23], demonstrating that RANS/LES has good capabilities to model turbulent flow fields while being less computationally expensive than full LES.
A simulation of plate-finned heat sinks shows that the RANS algebraic turbulence model was not able to predict the temperature of the heat sink due to the turbulence model adding excessive diffusivity and, therefore, underpredicting the surface temperature while LES provided acceptable results [24]. The accuracy of multiple RANS turbulence models was investigated by Weihing, Younis & Weigand [25]. They used the most common high Reynolds number turbu-

lence models and compared them with two low Reynolds number models. It was found that the low Reynolds number models that resolve to the wall are superior to models that use a wall function. The Reynolds-stress transport model was able to provide the most accurate results [25]. Combining the low-Reynolds number models with a Yap correction increases their accuracy and should be used for complex flows with heat transfer [26].

Using LES for flow simulation over a cube at a higher Reynolds number, Lodh, Das and Singh, 2017 [27] have shown that LES may be preferred over URANS. LES can capture most of the turbulent flow and turbulent kinetic energy accurately. For complex geometries, such as perforated fins, LES methods demonstrate an even more advanced ability to predict turbulent flow and heat transfer compared to RANS methods.
This is especially true for turbulent structures, such as recirculation zones, reversed flow zones and reattachment areas, where LES techniques provide more accurate results [28]. LES results seem to be more accurate for complex flow features, within 10% of experimental values [24]. NLES is a LES run without a turbulence model as explained in [29]. However, the different LES turbulence models are more consistent with each other due to a lower turbulence modelling difference. More details on LES and turbulence modelling can be found in [30, 31, 32] and for recent developments see [33]. The LES computational time can be substantially decreased with improved CPUs and parallel computing capabilities [34].

Direct numerical simulation (DNS) is the most accurate, but also the most expensive CFD method. This directly solves the Navier–Stokes equations in discrete form, offering very detailed and accurate information on the flow. It requires a very small grid spacing and timesteps, which increases the computational time significantly, scaling the cost of the simulation at Re^3, compared to LES (Re^2) and hybrid LES-RANS Re^1 [35]. DNS is not widely used due to its high computational cost compared to RANS or LES, but with increased

computing power, it will become an important tool [35].

2. Case setup

Due to lack of attached boundary layer flow and low Reynolds numbers indicating a lack of turbulence scale separation [32], we choose to contrast LES and NLES models with typical RANS modelling for the flow over a cube, representative of an electronic chip [36] and Aeroengine turbine blade cooling [7], [8]. The numerical LES (NLES) without subrid scale model was tested to asses the input for low *Re* flows. .

2.1 Geometry.

The wall-mounted cube matrix is the simple geometric structure of multiple cubes that are placed in regular intervals in a duct. To reduce the computational cost of the simulation, a sub-channel that includes one cube was modelled with periodic boundary conditions, representing a matrix of cubes. The flow domain is a duct with the dimensions of 0.06 m x 0.051 m x 0.051 m. The cube is placed in the centre of the domain, and its dimensions are 0.015 m x 0.015 m x 0.015 m. The outer layer of the cube is made from an epoxy material with a thickness of 0.0015 m, which is placed over a copper core. The height of the cube is denoted with H.

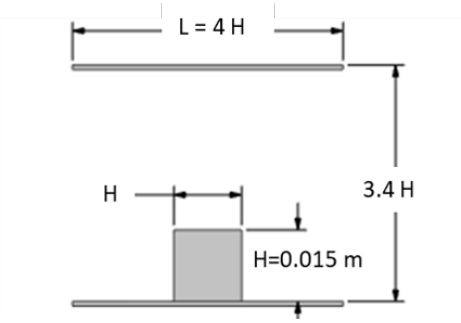

Figure 1: Sketch of flow domain.

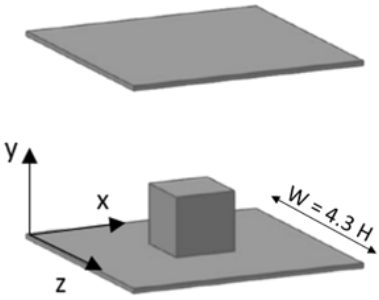

Figure 2: 3-D view of flow domain.

2.1 Boundary conditions and mesh.

The bulk flow has a velocity of $U_B = 3.86$ m/s which corresponds to a Reynolds number ($Re = \frac{\rho u_B H}{\mu}$) of 13,000. The flow field is periodic in the streamwise

and spanwise directions, which creates a matrix of cubes. The mass flow rate of 0.0137 kg/s is enforced by imposing a pressure gradient that is calculated at every timestep.

The copper core is subject to a constant surface temperature at 75 ˚C. The heat diffuses through the epoxy layer via conduction. The conductive heat transfer is significantly slower than convection; therefore, for the first 55 seconds, an implicit temporal scheme was used to increase the timesteps to 0.003 seconds. The density and thermal conductivity of the epoxy layer is 1150 kg/m^2 and 0.236 W/mK. The air at the inlet is 20 ˚C and has a density of 1.16 kg/m^3, a viscosity of 4.18e-6 m^2/s and a thermal conductivity of 0.026 W/mK. Since only one cube is heated, the temperature is set to 20 ˚C at the inlet and this is the only parameter that is not periodic in the streamwise direction. Aside from the cube, all walls are adiabatic,impermeabile and subject to a no-slip conditions. Once the temperature field in the epoxy layer was developed, the calculations were performed using a central differencing scheme and with a time step of 0.00005 seconds for LES. A mesh with 75 x 76 x 75 nodes was used. The RANS results were compared to a finer mesh with 109 x 109 x 109 nodes, this mesh reduced the surface temperature error by only 0.9 percentage points, compared the coarser mesh used. Additionally, any further reduction in time step size led to no further change in surface temperature or velocity profiles predictions of the RANS model. For the LES, the time step size has lead to a Courant-Friedrichs-Lewy condition of less than 0.7. The mesh is stretched towards the duct walls and cube, achieving an average wall distance of y^+=1.75. Seven nodes were placed inside the epoxy layer which are used to calculate the conductive heat transfer.

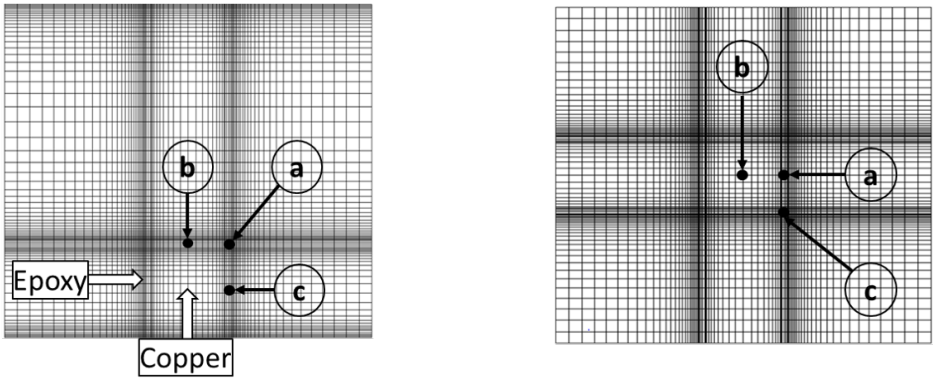

(a) (b)

Figure 3: Mesh in the a), x-y and b), x-z plane with indicators for conjugate temperature position.

Figure 3 shows the grid used in the computation, the letters indicate the locations where the temperature development in the epoxy layer was recorded as seen in Figure 4 and Table 1 shows the exact position of the recoding.

Position	x/H	y/H	z/H
a	2.49	0.99	1.5
b	2.00	0.99	2.0
c	2.49	0.54	2.0

Table 1: Position of the temperature recordings in epoxy layer. The cube heigh H can be replaced with the heights h_1 or h_2 for the additional cases described in section 5.

3. Numerical modelling

3.1 Boundary conditions and mesh.

The governing equations used to describe the flow field are the time-averaged (RANS) or filtered (LES) incompressible Navier-Stokes equations in Eqs.1 , 2.

$$\frac{\partial \widetilde{u_j}}{\partial x_j} = 0 \tag{1}$$

$$\rho\left(\frac{\partial \widetilde{u}}{\partial t} + \frac{\partial(\widetilde{u}_i\widetilde{u}_j)}{\partial x_j}\right) = \delta_{1j}\beta - \frac{\partial \widetilde{p}}{\partial x_j} + \frac{\partial}{\partial x_j}(\mu_{eff}\frac{\partial \widetilde{u_i}}{\partial x_j}) \tag{2}$$

These two equations are discretised using a finite volume formulation. The two turbulence modelling methods used are Reynolds Averaged Navier-Stokes and Large Eddy Simulation. The tilde symbol over u and p represents either LES or RANS variables. The LES variables are spatially filtered, while the RANS variables are time averaged. In equation 2, β is the mean pressure gradients. This mean pressure gradient enforces the mass flow rate and it is calculated at every time step using equation 3.

$$\beta_{new} = \beta_{old} - \rho\frac{(Q_{new} - Q_0) - 0.5\,(Q_{old} - Q_{new})}{0.5\Delta t H z_{max}} \tag{3}$$

Here, the volume flow rate and cross sectional area of the channel is denoted with Q_0 and Hz_{max} respectively. For every new time step, a new pressure gradient is evaluated which is denoted with subscript 'new'.

The anisotropic stress tensor is defined as:

$$\tau_{ij} = 2\mu_t\widetilde{S}_{ij} - \frac{2}{3}k\delta_{ij} \tag{4}$$

where $\widetilde{S}_{ij}$, k and δ_{ij} is the mean rate of strain tensor, the turbulent kinetic energy and Kronecker delta respectively. Hence $\mu_{eff} = \mu + \mu_t$ in equation 2.

3.2 Turbulence modelling.

To obtain the Reynolds stresses τ_{ij} in the RANS formulation, the Launder-Sharma Turbulence model [37] model was used. This model is a low Reynolds

number k-ϵ model which uses the Boussinesq approximation, which assumes that the Reynolds stresses are proportional to the mean rate of deformation [35]. To improve the accuracy of the model, the Yap correction was used [38]. The LES Subgrid-scale (SGS) stresses τ_{ij} modelled using the Yoshizawa SGS model [39]. In addition to the Yoshizawa SGS model, a Numerical LES (NLES) model was used which runs without an explicit SGS model. For the Yoshizawa model, the filter cut-off width was chosen to be proportional to the mesh size Eqn.5.

$$\Delta = (\Delta x \Delta y \Delta z)^{1/3} \tag{5}$$

2.3 Heat transfer modelling.

The heat transfer in the solid region of the cube was calculated using the conjugate heat transfer equation.

$$\rho \, C_p \frac{\partial \, T}{\partial \, t} = \frac{\partial}{\partial \, x_j} \left(k_{eff} \frac{\partial \, T}{\partial \, x_j} \right) \tag{6}$$

The eddy diffusivity model was used in the heat transfer calculations. The effective thermal diffusivity of the flow can be obtained using Eqn. 7.

$$k_{eff} = \frac{\mu \, C_p}{Pr} + \frac{\mu_t \, C_p}{Pr_t} \tag{7}$$

The turbulent Prandtl number is taken as 0.6 for LES and 0.9 for RANS. The temperature field within the fluid is then calculated using the temperature equation.

4. Results

4.1 Flow development and time independence.

The conductive heat transfer inside the epoxy layer takes a long time to develop. The flow through time ($T_L = \frac{L}{u_B}$) is $\mathrm{T_L} = 0.0155$ seconds, this is used to analyse the temperature development in three points of the epoxy layer which is plotted in Figure 4.The NLES surface temperature shows a fluctuating component due the turbulent flow over the cube. As seen in Figure 4a, position a takes the longest to reach the quasi-steady-state condition, therefore, a running average of 5 $\mathrm{T_L}$ was taken at position a. The quasi-steady-state condition is reached when $T = 0.99T_{final}$ where T_{final} is the last 5 $\mathrm{T_L}$ average recorded. For position a, it took 1783 $\mathrm{T_L}$ for the temperature to reach the quasi-steady-state condition, the other two positions reached this condition sooner.

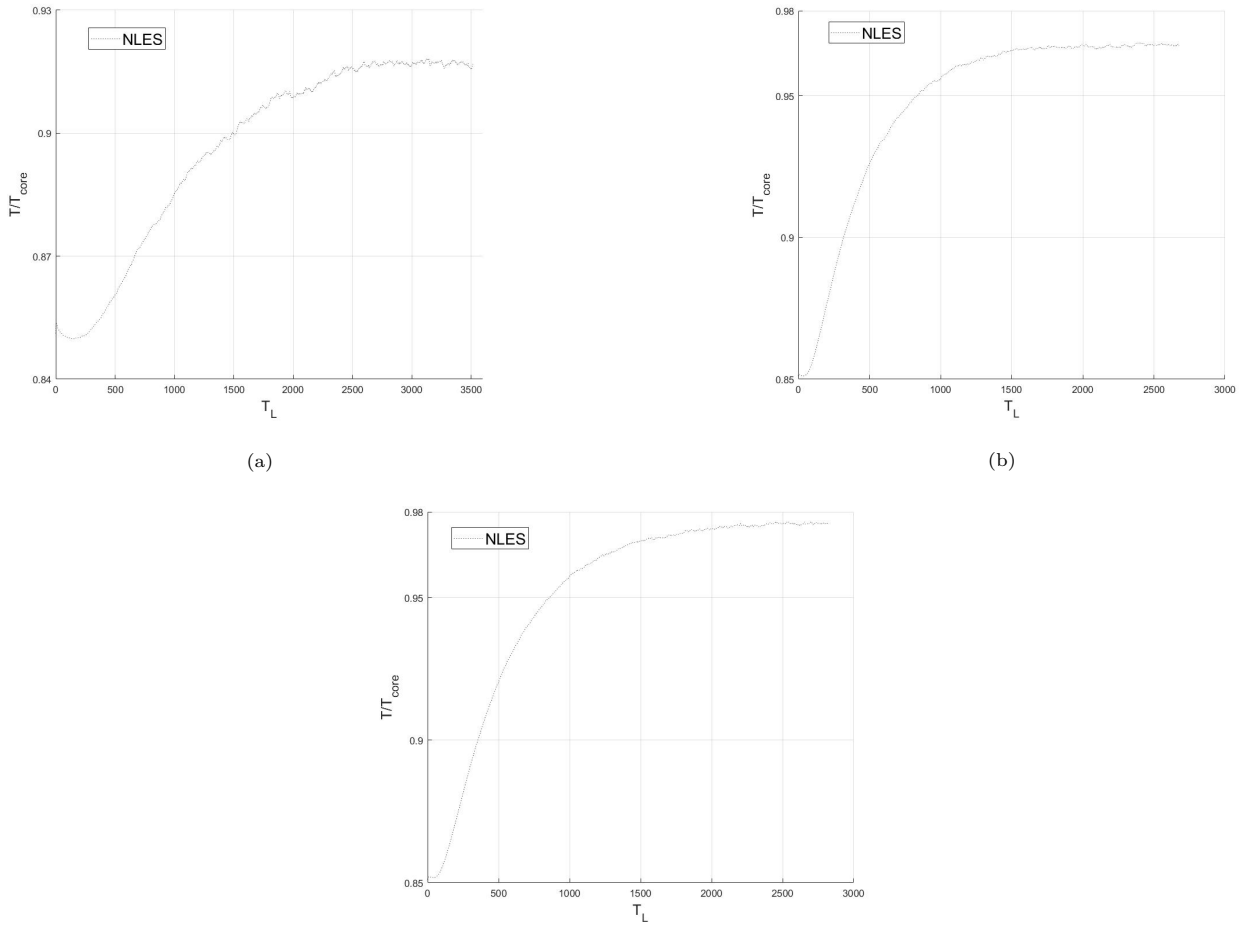

Figure 4: Temperature development of different points in the epoxy layer as shown in Figure 3 and Table 1.

To ensure that the time averaging includes enough time-dependent fluctuations and that the flow is fully developed, the averaged velocity profiles (u at x/H=2 and z/H=2) for different time intervals were compared. A benchmark run of 386 T_L was used to compare other averages against. Figure 5 shows the percentage difference of a streamwise velocity profile between the benchmark and a run with a smaller time average. The solution will become more accurate

as longer time-frames are induced in the avenging. Averaging the velocity field over different time intervals has shown that if the flow field is averaged over more than 150 T_L , the velocity profiles remain the same and the percentage error to the benchmark is less than 1 percent. This shows that enough turbulent structures are included such that averaging over a longer timeframe does not change the time-averaged parameters significantly and the flow has reached statistical stationary conditions.

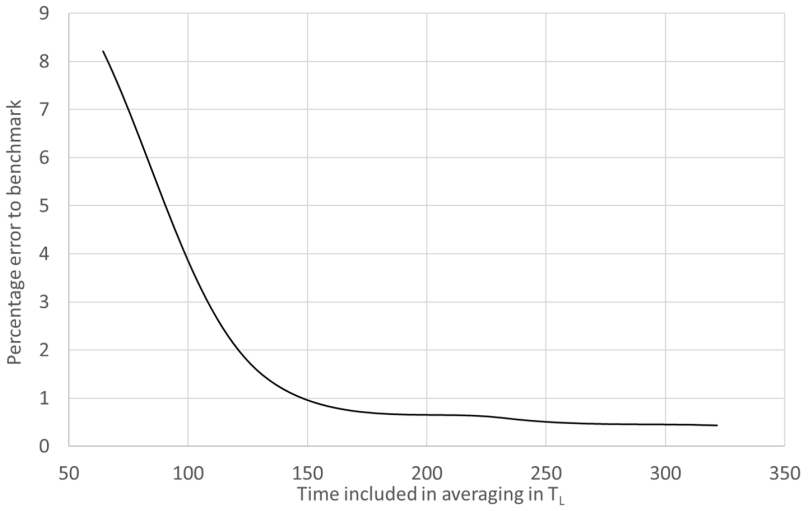

Figure 5: Percentage difference for solution with different averaging times to benchmark

Hence, the temperature field takes 11.9 times longer to develop than the velocity field. With no solution acceleration, a minimum of approximately 1800 T_L is required for flow development and 150 T_L for collection of statistics.

4.2 Key flow features.

The instantaneous flow field is highly time dependant and shows turbulent motions in a range of time and space scales. The dominating turbulent structure in front of the cube is a horseshoe vortex which forms just upstream of the cube. This horseshoe vortex is generated periodically and then breaks down due to the instabilities in the flow. The flow separates from all edges of the cube causing

instabilities in the flow which initializes vortex shedding. The instantaneous flow field for the LES (Figure 6), show the vortex shedding from all sides of the cube and a Kármán vortex street that is formed in the wake of the cube. The RANS model (Figure 7) is not able to predict such vortex shedding behaviour and the flow does not detach from the sides of the cube as it does in the LES.

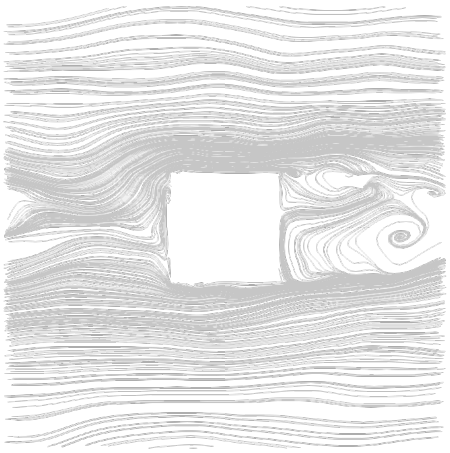

Figure 6: LES streamlines x-z plane, y/H=0.6

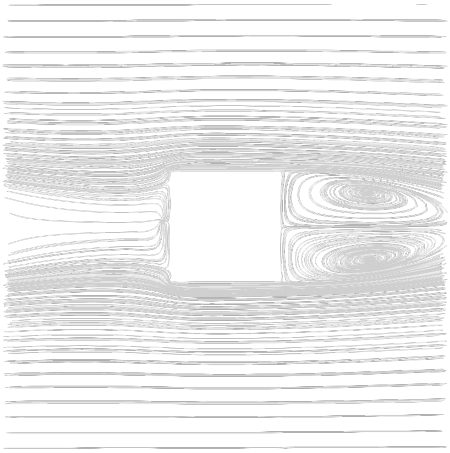

Figure 7: RANS streamlines x-z plane, y/H=0.6

4.3 Mean flow.

To compare the mean flow field, all parameters are averaged for at least 220 T_L. The time-averaged streamwise velocity component u is plotted at three locations along the centre line of the duct in Figure 8. It shows the velocity profile just upstream the cube, on the cube's top face and in wake of the cube. The streamwise velocity u is normalized by U_B. The obtained data was compared with the experiment conducted by [40] which is based on [41]. The average error between the experimental data and the CFD calculations was determined through a mesh-face weighted averaging. Equation 8 was used to calculate the error between simulation and the experiment, equation 9 was used to determine the average mesh-face weighted error over every velocity plot. In Equation 9 Δy_i is the size of the mesh element in y direction where the value was recorded.

$$\overline{error_i} = \left| \frac{100(u_{exp,i} - u_{CFD})}{u_{exp,i}} \right| \tag{8}$$

$$\overline{error} = \frac{\sum_{i=1}^{n} \overline{\text{error}_i} * \Delta y_i}{\sum_{i=1}^{n} \Delta y_i} \tag{9}$$

CFD variables are interpolated to the experimental measurement location. The overall error is an arithmetic mean of mesh-face weighted error over the three profiles.

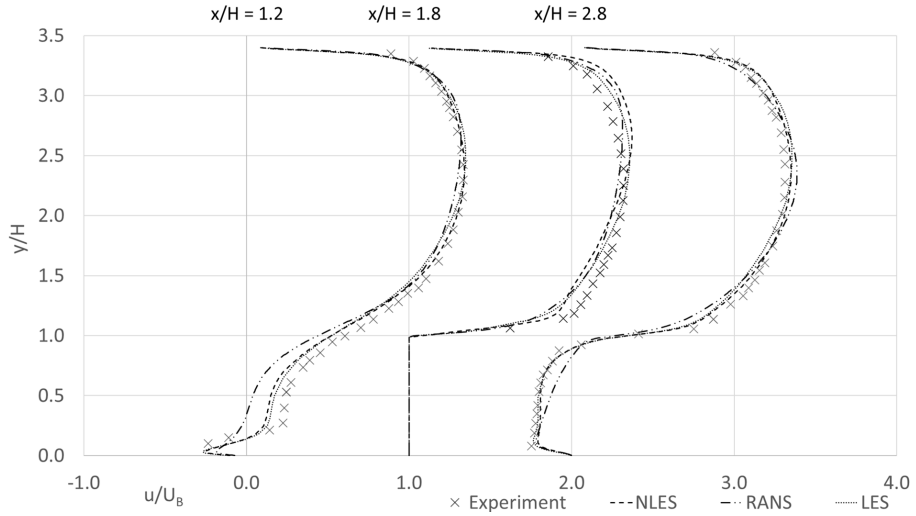

Figure 8: Streamwise velocity comparison

In Figure 8, at x/H=1.2, which is just upstream the cube, the RANS simulation underpredicts the negative flow velocity close to the wall drastically. The horseshoe vortex is located in the region between y/H=0 and y/H=0.25, which the RANS simulation was not able to accurately predict. Even above the horseshoe vortex, RANS was not able to represent the flow field up to y/H=1.5, which is close to the free stream. Both LES and NLES performed significantly better but they underpredicted the velocity profile close to the wall. Using the Yoshizawa SGS model increased the accuracy by a few percent. At x/H=1.2, the mesh-face weighted average error for the RANS is 20.5%, while the NLES model gives 10.0% error and the Yoshizawa SGS model performance the best

with 9.3% error. All models perform well in the free stream while having issues in accurately resolving the horseshoe vortex. This is likely due to more isotropic convected turbulence and lower streamline curvature in the free stream.

The velocity profile at x/H=1.8 is located on the top face on the cube. All models perform well in this region; the flow is accelerated in the streamwise direction with a high near wall velocity gradient. The RANS model has an error of 8.4%, while the NLES has an error of 6.7% and the LES model has 4.6% error. The wake of the cube is dominated by a large recirculation area which can be seen at x/H=2.8 by a large region with negative u velocity. RANS underpredicts the negative velocity in the wake of the cube while giving good results above y/H=1.5. The NLES showed a good capability of resolving the recirculation bubble. However, using an SGS model did improve the accuracy in this region with LES having an error of only 6.2%.

Overall, the RANS simulation has an error of 14.3%, while the NLES model has an error of 7.1% and the overall error of the Yoshizawa SGS model is 6.2%. The gap between RANS and LES is even wider if only the region between y/H=0 and y/H=1.5 is considered. In this region around the cube, using LES has more than halved the average error from 34.0% for RANS to about 15% for the LES with noticeable improvements using the SGS model. Is is more important to obtain the curved-flow near the walls in order to correctly predict the heat-transfer.

4.4 Reynolds stresses.

The time averaged streamwise and cross-stream velocity fluctuations <u'u'> and <v'v'> form part of the turbulent stress. The turbulent stresses have a strong effect on the heat transfer from the cube since turbulence increases thermal mixing. Therefore, it is vital for turbulence models to capture the turbulent stresses accurately since they will directly affect heat transfer prediction. The Reynolds stresses in Figure 9a and 9b are normalised by u_B^2. The Reynolds stresses <u'u'> and <v'v'> for the RANS simulation were calculated using the Boussinesq approximation.

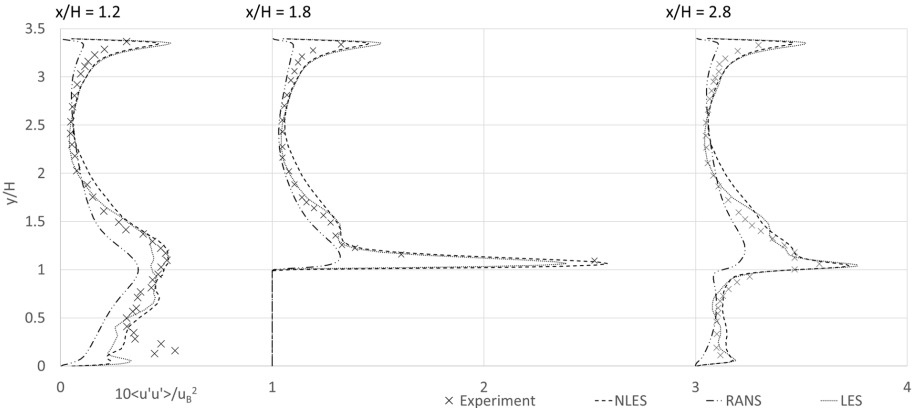

(a) Normalised resolved <u'u'>' stress

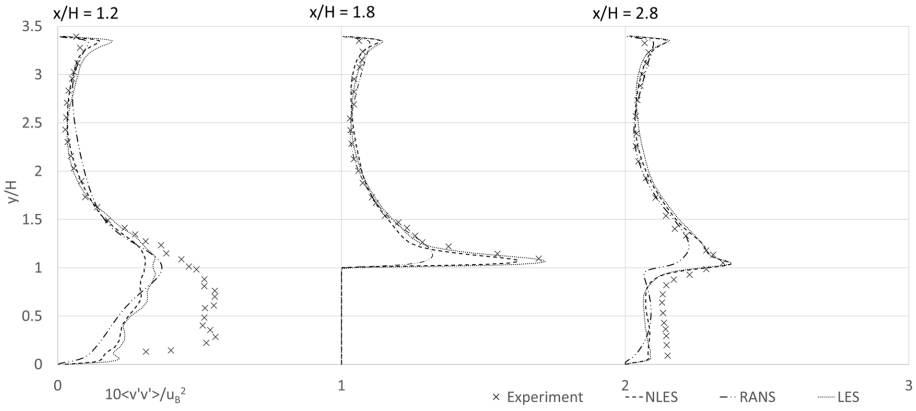

(b) Normalised resolved <v'v'> stress

Figure 9: Time averaged streamwise and cross-stream velocity fluctuations as three positions

In Figure 9a, the stresses in the streamwise directions are shown. The RANS simulation is drastically underpredicting the peaks in turbulent stresses caused by the shear layer at y/H=1.1. In the three positions, turbulent stress fluctuations are underpredicted in the important regions close to the wall and around the cube, while the free-stream turbulence is modelled with moderate errors. This leads to an overall error of around 34.0% for the RANS simulation.

The NLES model overpredicts <u'u'> in the freestream but it is much better in capturing the peaks in the shear layer. The stresses in the shear layer up

to y/H=1.5 are predicted with a significant increase in accuracy compared to the RANS simulation. Overall, the NLES error in <u'u'> is about 29.7%. The Yoshizawa model performed better than the RANS and LES, especially in the free stream region. This gives an overall error of about 21% for the LES model. Figure 9b shows the normalised cross-stream velocity fluctuations <v'v'>. At x/H=1.2 the all three models underpredict the velocity fluctuations up to y/H=1.3. This may show that the mesh around the cube is too coarse to capture the fluctuations far downstream of turbulence generation. The RANS model is again underpredicting the velocity fluctuations and is unable to capture the peak in the shear layer, with an average error of 35.4% up to y/H=1.5. The LES performs slightly better than the NLES, especially in the shear layer and upstream the cube.

Overall, the RANS simulation is unable to accurately predict the peaks in the turbulent stress in the shear layer and the near-wall region, but in the centre of the duct, it gives acceptable results. Both LES and NLES outperform the RANS simulation with a slightly improved result using the SGS model. The mesh weighted average error in the region from y/H=0 to y/H=1.5 are shown in Table 2.

	RANS x/H = 1.2	NLES x/H = 1.2	LES x/H = 1.2	RANS x/H = 1.8	NLES x/H = 1.8	LES x/H = 1.8	RANS x/H = 2.8	NLES x/H = 2.8	LES x/H = 2.8
u	55.09	27.04	22.43	16.52	10.91	10.69	30.12	7.50	6.25
<u'u'>	40.72	17.60	18.09	32.41	11.95	10.17	28.19	21.82	18.05
<v'v'>	46.91	41.92	37.84	25.44	18.10	8.19	34.04	33.16	39.68

Table 2: Area weighted average error in region from y/h = 0 to y/h = 1.5

4.5 Energy spectrum.

The Energy spectra at three locations in the flow domain were calculated using a Pwelch Fourier Transform. The locations of the three positions are denoted in Table 3 and Figure 10 visualizes the locations of the energy spectrums in

the domain. Figure 11 shows the instantaneous velocity profile which shows the scale of the turbulent structures behind the cube.

Position	x/H	y/H	z/H	$\Delta x/H$	$\Delta y/H$	$\Delta z/H$
1	1.20	0.12	2	0.0339	0.0179	0.0890
2	2.31	1.16	2	0.0603	0.0216	0.0816
3	2.67	1.07	2	0.0394	0.0303	0.0890

Table 3: Locations of recorded energy spectrums and size of mesh

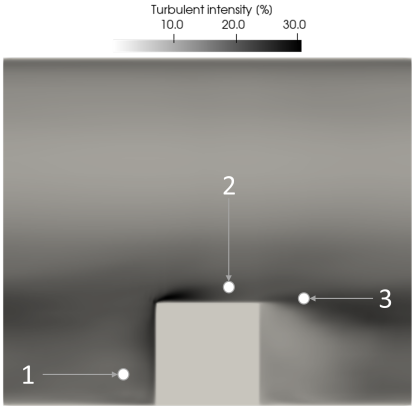

Figure 10: Turbulent intensity with indications of positions of energy spectra's

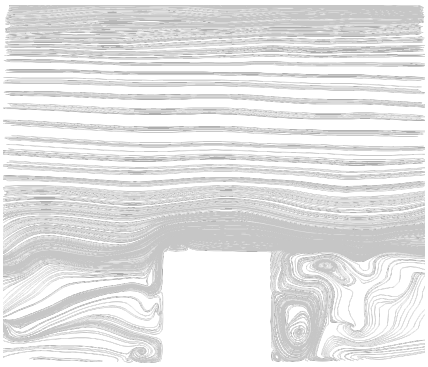

Figure 11: LES instantaneous streamlines x-y plane, z/H=2

To obtain a relevant turbulence time scale, the flow time over the cube $T_H = H/U_B = 3.889 \times 10^{-3}$ seconds is used. For the calculation of the energy spectra, a time sample of at least 1544 T_H was used. Reducing the size of the recorded flow data has shown that the peak of the spectrum will change when the length of the recorded data falls below 100 T_H which corresponds to approximately 23 T_L. This indicates a lower bound for data recording to obtain low frequencies (large scales).

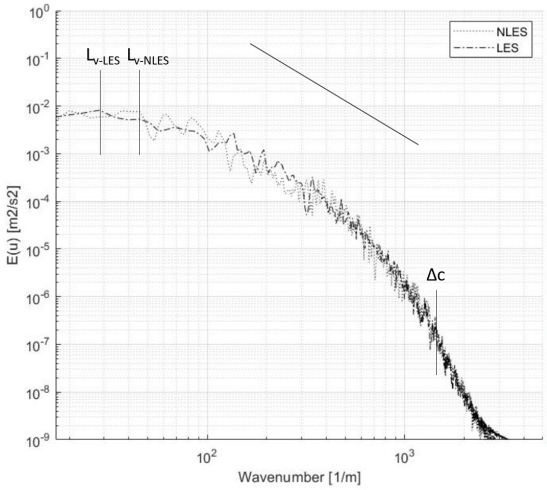

(a) Position 1

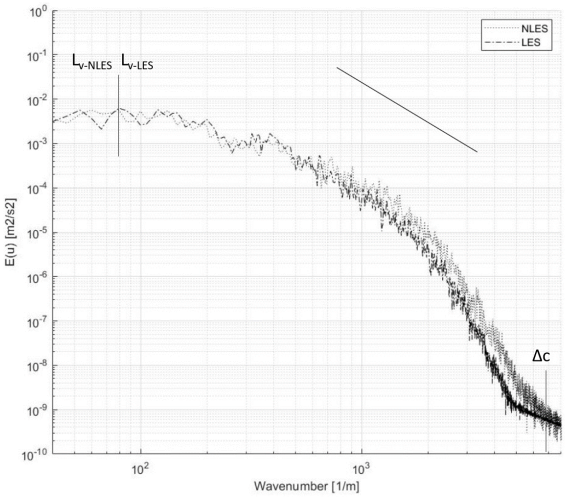

(b) Position 2

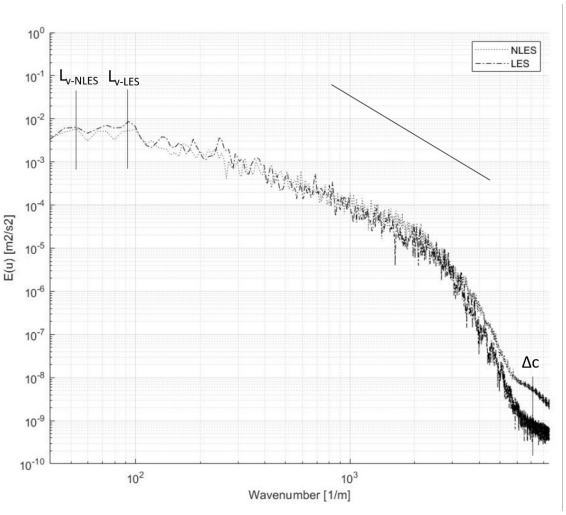

(c) Position 3

Figure 12: Energy spectrums for NLES and LES for all three locations with locators for maximum energy L_v and mesh cut off wavenumber Δc. The back line above the spectrum indicates the -5/3 slope of the isotropic turbulence/Kolmogorov spectrum.

As seen in Figure 12, the energy spectrums contain a relatively small -5/3 region for the NLES and LES. The peaks in the LES energy spectrum shows the size of the largest eddies present in the flow. The corresponding eddy sizes

are given in Table 4.

Model	Position	Largest scale L_v [m]	Normalised scales L_v/H
NLES	1	0.0271	1.81
LES	1	0.0352	2.35
NLES	2	0.0126	0.84
LES	2	0.0126	0.84
NLES	3	0.019	1.26
LES	3	0.0108	0.71

Table 4: Size of the largest eddies

Position 1 is located in the wake of the cube, therefore, the largest scale L_v is bigger than right behind the cube. The normalised scales show that the largest turbulent structures in the developing shear layer, behind and above the cube (Position 2 and 3), are of a smaller size than cube. This shows that the size of the largest eddies in the flow is smaller than the obstacle dimension. This is useful to determine the mesh resolution requirements downstream.

The largest turbulence scales L_v are roughly the size of H, while the smallest scales are η (Kolmogorov length scale). Calculating the Reynolds number using the cube size H as the characterise length, one can obtain the Reynolds number $\mathrm{R_H} \approx 3800$. The length scale ratio L_v/η can be calculated using equation 10:

$$\frac{L_v}{\eta} = {R_H}^{0.75} \tag{10}$$

This yields a theoretical length scale ratio of $L_v/\eta \approx 500$ which means that the smallest scales are approximately the size of $L_v/500$. For a substantial inertial subrange to exist it requires a ratio of 1000 or more [42].
The NLES spectrum for point 3 Figure 12c shows a minimum wavenumber of 50 and a filter cutoff wavenumber of approximately 7539, which can be used to obtain a length scale ratio of $L_v/\Delta c = 150.8$. Some scales will be unresolved

due to the grid filter width.

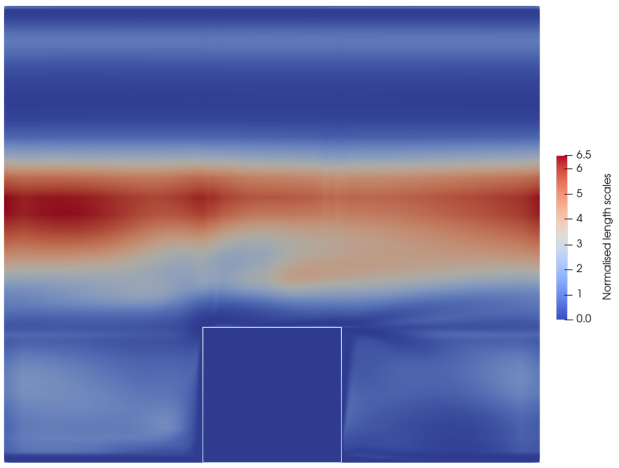

Figure 13: Normalised length scales RANS, z/H=2

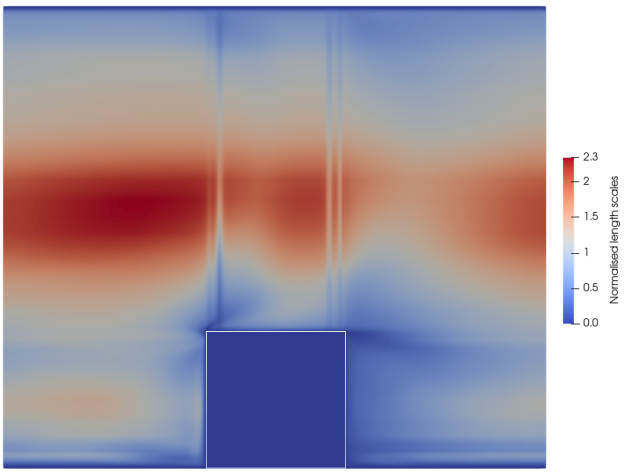

Figure 14: Normalised length scales LES, z/H=2

Figure 13 and 14 show the normalised length scales (L_v/H) through the domain. RANS ($L_{v-RANS} = \frac{\kappa^{3/2}}{\epsilon}$) predicts large length scales in the middle of the domain of more than $L_{v-RANS}/H = 6$, while the NLES predicts a maximum normalised length scale of $L_{v-NLES}/H = 2.3$. Table 5 shows the normalised length scales obtained from the calculations at the three points. At position 1 and 2, the calculated length scales for NLES and LES are significantly smaller than those obtained from the energy spectrum (table 4). At position 3, they seem to show similar values for $L_{v,LES}/H$.

Postion	NLES	LES	RANS
1	0.39	0.40	0.24
2	0.47	0.55	0.74
3	0.91	0.93	1.13

Table 5: Calculated normalised length scales L_v/H for the three models

4.6 Surface temperature.

Two temperature profiles along the two lines shown in Figure 15 are presented in Figure 16 and 17.

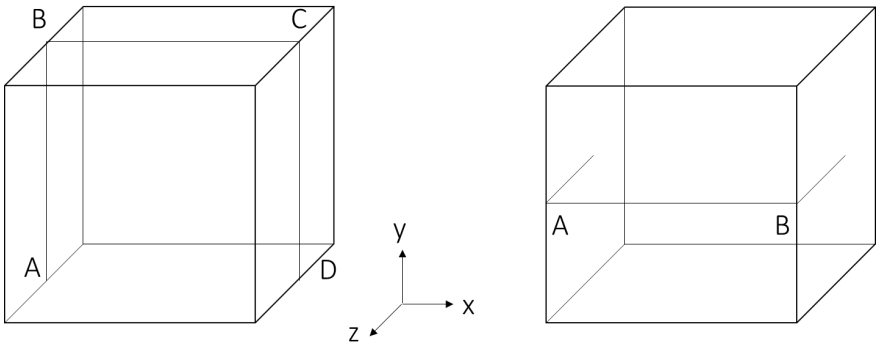

Figure 15: Visualisation of surface temperature profiles on the cube

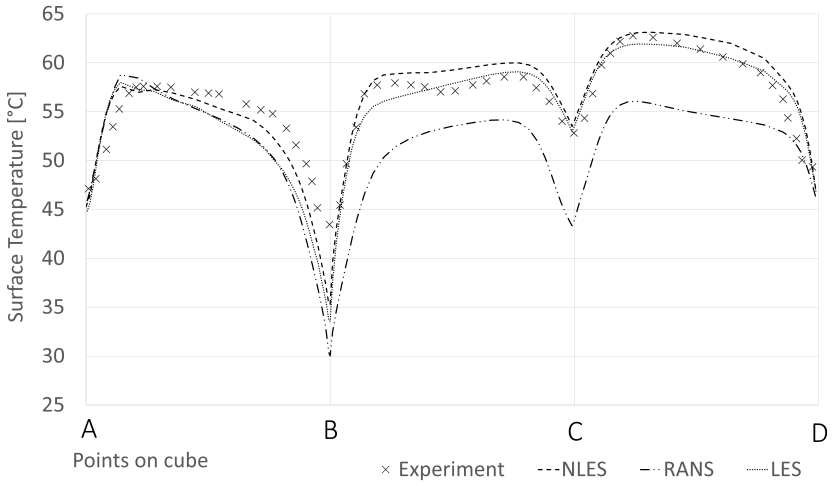

Figure 16: Comparison of surface temperature along constant z line

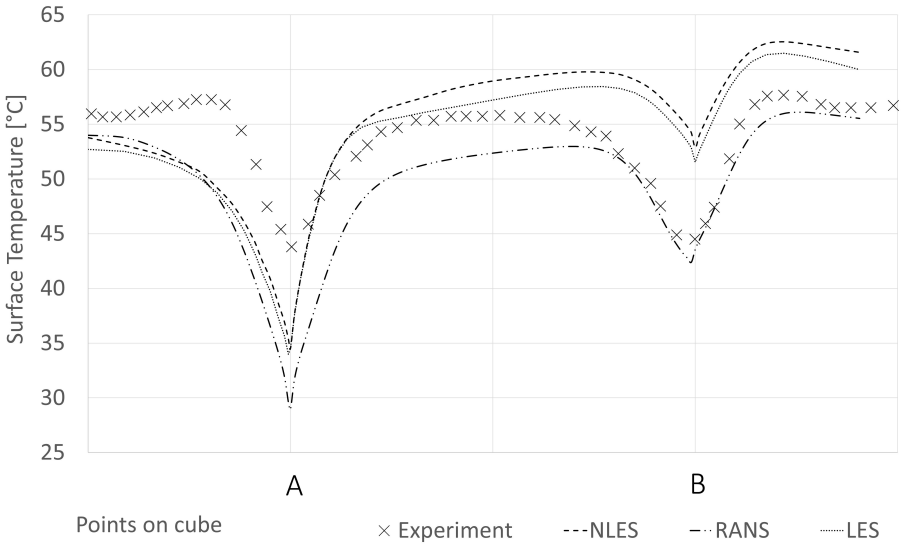

Figure 17: Comparison of surface temperature along constant y lines

In Figure 16 and 17, a lower surface temperature means a higher heat transfer coefficient. The sharp drop in surface temperature on the edges of the cube is due to an increase in heat transfer coefficient on the edges. More heat is removed from the edges because of the exposure to cold fluid on two faces and the turbulence created around the edges. The temperature of the front face of the cube is slightly lower than the side or the top faces due to the impingement flow which increases the heat transfer on this face.

The RANS model surface temperature prediction is accurate with an average error of 5.7% for the constant y profile and 9.1% for the constant z profile. However, since the flow field and velocity fluctuation, especially around the cube, have quite high errors, it seems like these results are more fortuitous and do not seem to agree with the other data obtained from the RANS simulation. Since this flow can be classified as a top-down flow, where the large turbulent structures are more important to resolve for the heat transfer, it is surprising that the RANS model was able to accurately predict the surface temperatures without resolving the complex time-dependent features.

The NLES model performs better than the RANS, with an error of 7.7% for the constant y profile and 2.4% for the constant z profile. It slightly overpredicts the surface temperature along the constant y profile. It seems to be challenging for all models to predict the surface temperature at the front face of the cube due to the complex horseshoe vortex present at this face as well as interactions with the modelled wake flow from upstream cubes. However, along the edges of the cube, LES performs better than the RANS simulation due to its improved ability to better resolve the anisotropic turbulence around the edges. The LES obtains slightly better balanced results than the NLES, with an average error of 6.4% for the constant y profile and 3.1% for the constant z profile. It seems that using the one equation SGS model does not significantly improve the heat transfer predictions. This might be because the increase in accuracy in the flow field and turbulence predictions are not significant enough to further enhance the thermal predictions or that the eddy-diffusivity model and the use of a constant turbulent Prandtl number for modelling is the restricting factor which would make further improvements in turbulence models unnecessary.

5. Cube height effect

Now that all three models have been validated against experimental results, two new cases with different cube heights are investigated. The two new cube heights, h_1 and h_2, are of size $h_1/H = 1.5$ and $h_2/H = 0.5$ respectively. All boundary conditions remain the same, the only difference is the mesh. For the two new cases, the mesh in the y direction was changed to reflect the different heights of the cube. The mesh in the x and z directions remained the same. The two new meshes both have 75 x 76 x 75 nodes, with a similar resolution as the baseline case. Figure 18 shows the two new domains and meshes.

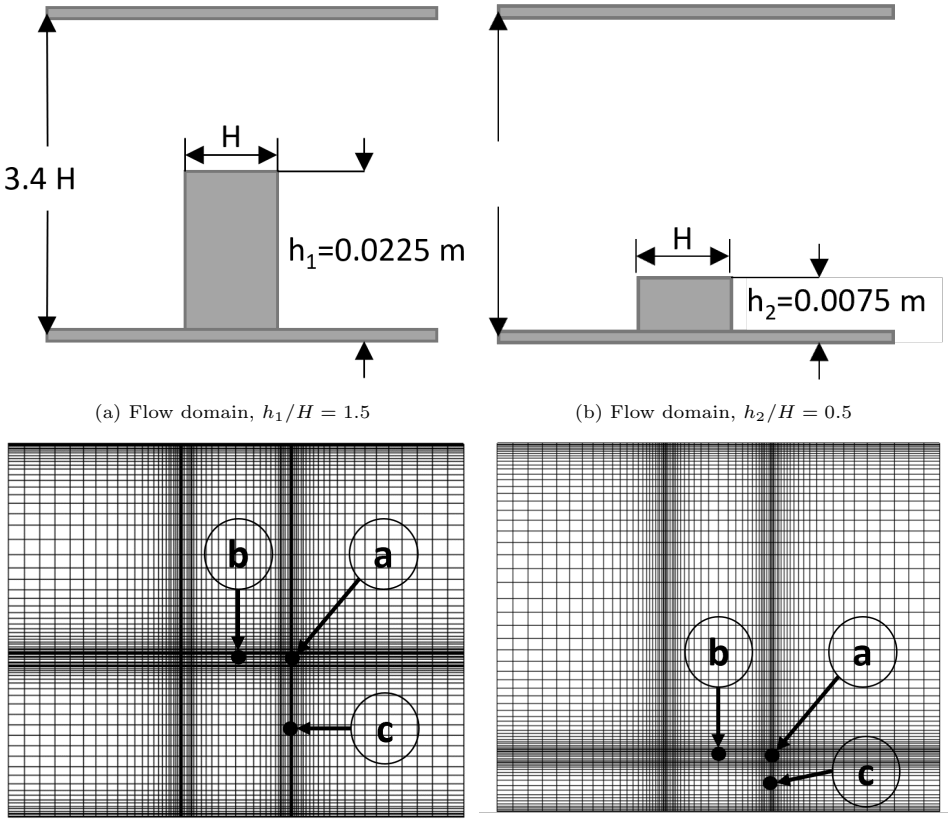

(a) Flow domain, $h_1/H = 1.5$

(b) Flow domain, $h_2/H = 0.5$

(c) Mesh of h_1 case

(d) Mesh of h_2 case

Figure 18: Flow domains and meshes for new cube heights

The three locations reporting the temperature development remained the same in the x and z locations but the y location have moved in respect to the new cube heights, Table 1 also shows the new y position, relative to the new heights (h_1 and h_2).

As the cube gets smaller, the time it takes to reach the quasi-steady-state condition takes longer. For the cube heights of h_1 and h_2, the maximum time taken to reach 99% of the final temperature is 1756 T_L and 2148 T_L respectively. Figure 19c shows the development of the epoxy layer temperature of the three points.

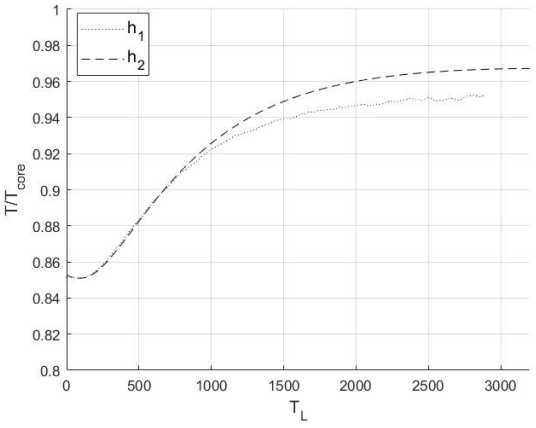

(a) Position A

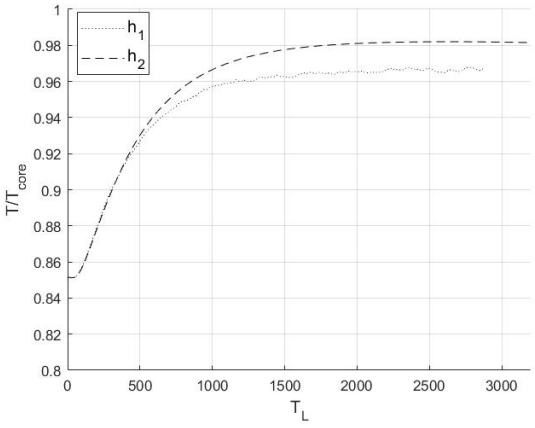

(b) Position B

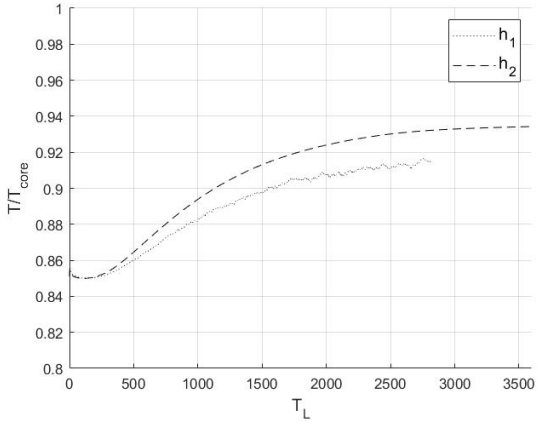

(c) Position C

Figure 19: Temperature NLES development of points in epoxy layer

The two cases were run until the temperature field was fully developed and the time dependant statistics were averaged over more than 150 T_L. The time averaged streamwise velocity and velocity fluctuations for both cases are shown in Figure 20, the first row shows the case h_1. Increasing the cube height leads to an increase in the discrepancy between the three models, especially in the time averaged streamwise velocity fluctuations. The <u'u'> peaks in the shear layer show a significant difference between the models. RANS underpredicts

the free stream velocity and shows a significantly different flow profile in the recirculation bubble. Both LES models are in good agreement with each other for the area below the cube ($y/H < 1.5$). The bottom row of Figure 20 shows case h_2. In this case, the predictions of the models are similar, especially for the flow field. RANS still underpredicts the velocity fluctuations around the cube but the velocity field in the recirculation bubble is in better agreement with the LES data.

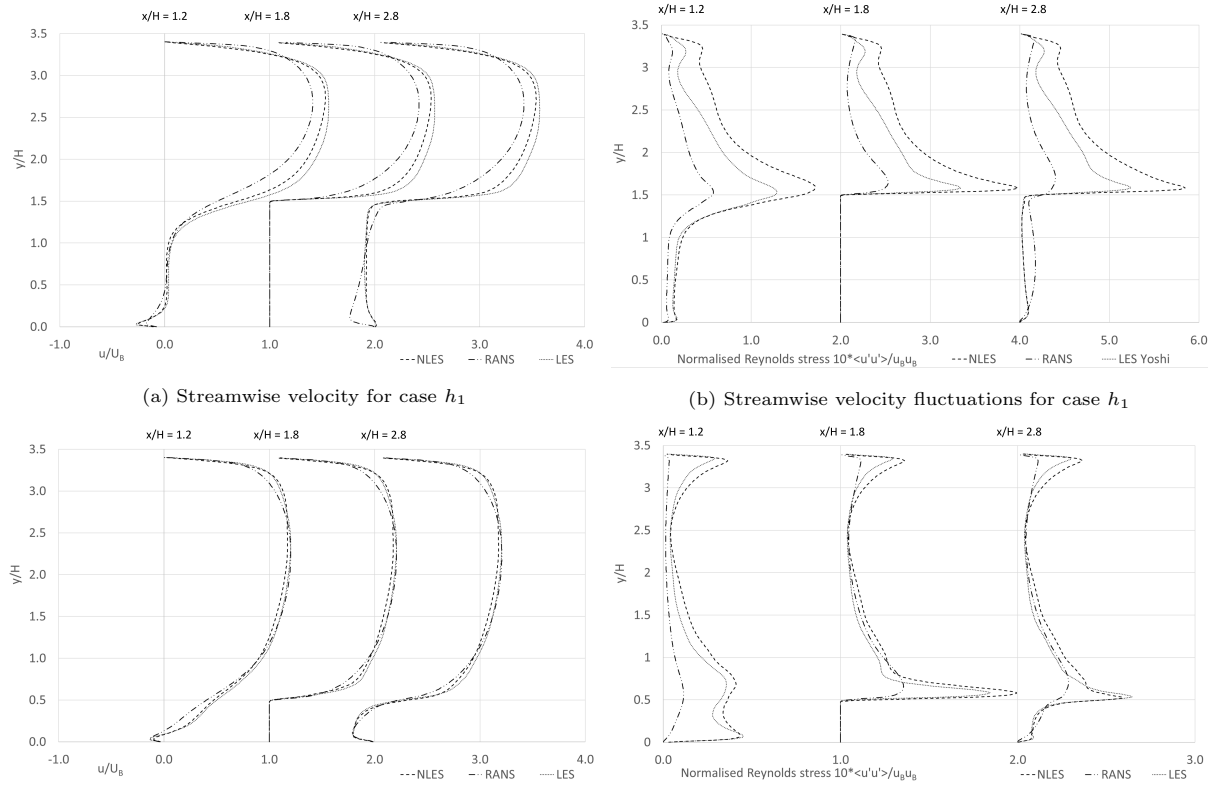

(a) Streamwise velocity for case h_1

(b) Streamwise velocity fluctuations for case h_1

(c) Streamwise velocity for case h_2

(d) Streamwise velocity fluctuations for case h_2

Figure 20: Time averaged streamwise velocity and velocity fluctuations for three positions

The resultant surface temperature for both cases is shown in Figure 21. This figure shows the surface temperature for the three models along the constant z and y lines, similar to the lines shown in Figure 15. However, the constant y lines are located in the middle of the cube height, $y/h_1 = 0.5$ and $y/h_2 = 0.5$

respectively, the constant z lines start and end at this height as well.

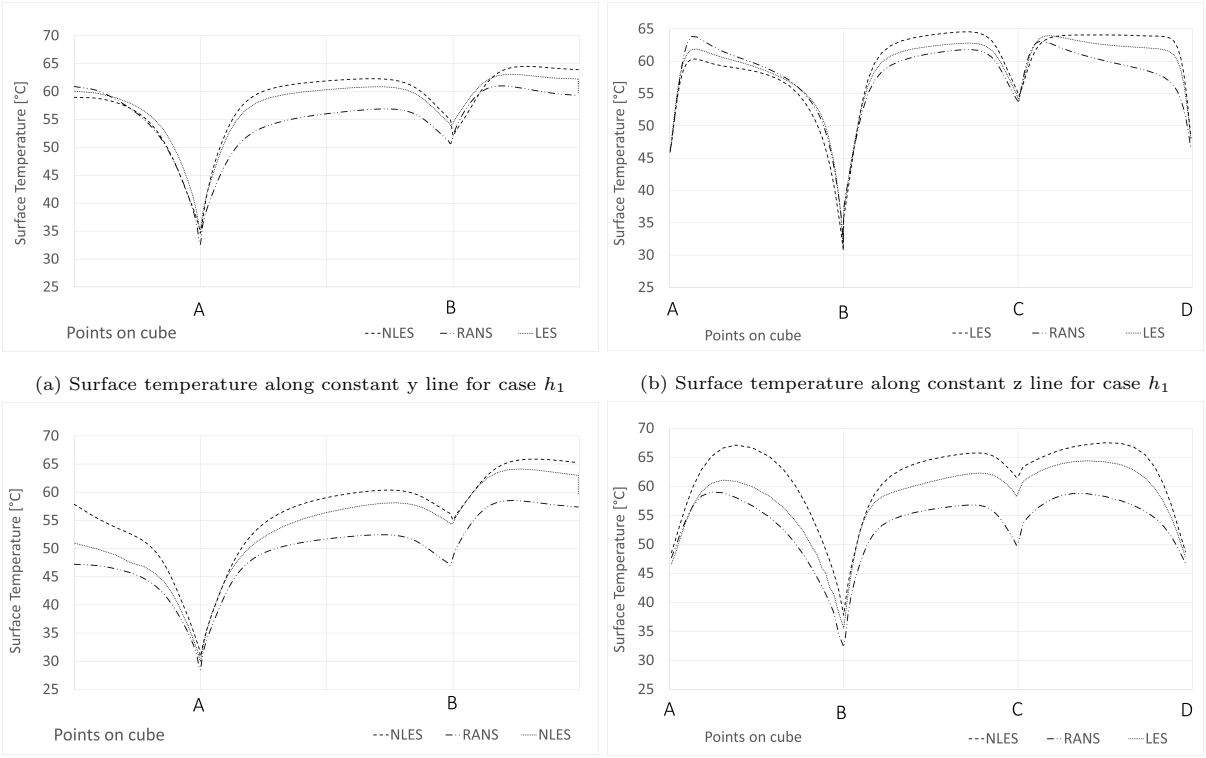

(a) Surface temperature along constant y line for case h_1

(b) Surface temperature along constant z line for case h_1

(c) Surface temperature along constant y line for case h_2

(d) Surface temperature along constant z line for case h_2

Figure 21: Surface temperature plots for the two cases

The first row of surface temperatures are for case h_1. The increased turbulent flow has lead to a larger difference between the three models. Comparing the h_1 case to the base case, the average temperature difference between NLES and LES had increased by more than 30%. RANS is again predicting a lower surface temperature than the LES models. The second row in Figure 21 shows the surface temperature for the smallest cube. For this case, the models show a wider variety of temperature predictions. This is because the profiles were extracted in a sensitive region due to the profiles being near the edge of the horseshoe vortex. This is supported by the case h_1 profiles being located above the horseshoe vortex which leads to them being more consistent with each other.

6. Computing time

The simulations presented in this report were run on a single core of a CPU. The time to complete the simulation varies significantly among the three models tested. The RANS model is able to converge in a matter of hours depending on its initial condition while both LES have turnaround times of a one day. The Numerical LES is 15% faster than the Yoshizawa model since it lacks a turbulence model which means that it does not solve any additional transport equations apart from the Navier-Stokes equations.

7. Conclusion

The heat exchange between roughness elements and air is a complex system that is difficult to model with a high degree of certainty. In the cases discussed in this project, the RANS heat transfer predictions vary from average errors of 9.1% to 5.7%. However, RANS inability to resolve turbulent structures and significant errors in the velocity field and turbulence make it less reliable and results should be used with caution. RANS can be unpredictable for use in modelling heat transfer due to its inability to reliably model turbulent structures. Additionally, the RANS model's tendency to overpredict heat transfer is a major problem because it could mean that cooling systems developed using the model may not sufficiently dissipate the produced heat. The resulting increase in thermal stress on the components can make them more prone to failure. Knowing that the RANS model may be overestimating heat transfer, oversizing the cooling systems may be a solution for non-critical components (e.g. in personal computers or devices with low thermal loads).
However, in areas like the aerospace industry, where electronic components and aeroengine turbine blade cooling are major safety concerns and where small safety factors prevent the oversizing of the heat exchange systems due to weight restrictions, oversizing the system may not be possible. In these cases, it is important to accurately predict the heat dissipation of the thermal management

system. Hence, LES is the preferred choice because it can predict the heat transfer coefficient more accurately with a turnaround time of one day. Not using an SGS model may increase the speed of the simulation, but it slightly decreases the heat transfer modelling capabilities. The NLES was able to predict the heat transfer with errors from 7.7% to 2.4%. This is a meaningful improvement over the RANS model. The Yoshizawa SGS model further improves heat transfer modelling by increasing the accuracy of the velocity field and turbulence modelling. The resulting error is between 6.4% and 3.1% in the cube matrix case. This small increase in the accuracy of the thermal predictions comes with a 15 % increase in run time compared to the NLES results. Therefore, the increase in accuracy may not warrant the use of the one equation model in this case. However, more complex geometries and coarse mesh may benefit from additional turbulence modelling.

Two cases with a cube height of 0.5 and 1.5 times the initial cube height were also investigated. The time taken for the cases to reach a quasi-steady state temperature field decreases with cube height. The temperature predictions for the smallest cube show larger differences between the models due to the complex flow structures where the profiles were extracted.

Additionally, the current study has provided quantitative data on how long such flows may take to develop and how long statistics need to be measured, this will be informative for future simulations. The flow needs to develop for approximately 1800 T_L and 150 T_L for collection of statistics is required. Energy spectra also identified significant range in turbulence length scales prediction between RANS and (N)LES. (N)LES scales appeared physically reasonable and should inform mesh resolution in future studies.

References

[1] Y. A. Çengel, A. J. Ghajar, Heat and mass transfer: fundamentals and applications, McGraw Hill Education, 2015.

[2] S. Bergstein, The influence of the operating temperature on the service life and reliability of switching power supplies - technical articles (2019). URL https://eepower.com/technical-articles/the-influence-of-the-operating-temperature-on-the-service-life-and-reliability-of-switching-power-supplies/

[3] S. Anandan, V. Ramalingam, Thermal management of electronics: A review of literature, Thermal Science 12 (2) (2008) 5–26. doi:10.2298/tsci0802005a.

[4] W. M. Adams, Power consumption in data centers is a global problem (Nov 2018). URL https://www.datacenterdynamics.com/opinions/power-consumption-data-centers-global-problem/

[5] C. Nadjahi, H. Louahlia, S. Lemasson, A review of thermal management and innovative cooling strategies for data center, Sustainable Computing: Informatics and Systems 19 (2018) 14–28. doi:10.1016/j.suscom.2018.05.002.

[6] C. Mayr, A. Traußnig, How to optimise thermal management for battery electric vehicles, AVL (2019).

[7] J. Tyacke, P. Tucker, Large eddy simulation of turbine internal cooling ducts, Computers and Fluids 114 (2015) 130–140. doi:10.1016/j.compfluid.2015.02.022.

[8] A. Beniaiche, C. Carcasci, M. Pievaroli, A. Ghenaiet, Nusselt correlations in a trailing edge cooling system with long pedestals and ribs, Energy Procedia 45 (2014) 1067–1076. doi:10.1016/j.egypro.2014.01.112.

[9] P. Rostek, G. Renouard-Vallet, Hybrid electric propulsion: technology bricks beyond mea hybrid electric propulsion (2015).

[10] S. Fletcher, M. Flynn, C. Jones, Hybrid electric aircraft: State of the art and key electrical system challenges, IEEE Transportation Electrification Community (Sep 2016).

[11] W. Rodi, Turbulence modeling and simulation in hydraulics: A historical review, Journal of Hydraulic Engineering 143 (5) (2017) 03117001. doi:10.1061/(asce)hy.1943-7900.0001288.

[12] K. Dhinsa, C. Bailey, K. Pericleous, Accuracy of turbulence models and cfd for thermal characterisation of electronic systems, Proceedings of the 5th Electronics Packaging Technology Conference (EPTC 2003) (2003) 507–512doi:10.1109/eptc.2003.1271573.

[13] K. Dhinsa, C. Bailey, K. Pericleous, Turbulence modelling for electronic cooling: A review, 2005 International Symposium on Electronics Materials and Packaging (2005). doi:10.1109/emap.2005.1598275.

[14] C. J. Lasance, C. Rindt, Accuracy comparison of a standard cfd code for the thermal analysis of non-simple geometries with baseline experiments, Twenty-Third Annual IEEE Semiconductor Thermal Measurement and Management Symposium (2007). doi:10.1109/stherm.2007.352432.

[15] S. Vijiapurapu, J. Cui, Performance of turbulence models for flows through rough pipes, Applied Mathematical Modelling 34 (6) (2010) 1458–1466. doi:10.1016/j.apm.2009.08.029.

[16] M. Caciolo, P. Stabat, D. Marchio, Numerical simulation of single-sided ventilation using rans and les and comparison with full-scale experiments, Building and Environment 50 (2012) 202–213. doi:10.1016/j.buildenv.2011.10.017.

[17] S. M. Salim, K. C. Ong, Performance of rans, urans and les in the prediction of airflow and pollutant dispersion, Lecture Notes in Electrical

Engineering IAENG Transactions on Engineering Technologies (2012) 263–274doi:10.1007/978-94-007-4786-9_21.

[18] Z. Yang, Assessment of unsteady-rans approach against steady-rans approach for predicting twin impinging jets in a cross-flow, Cogent Engineering 1 (1) (2014). doi:10.1080/23311916.2014.936995.

[19] S. Karabelas, B. Koumroglou, C. Argyropoulos, N. Markatos, High reynolds number turbulent flow past a rotating cylinder, Applied Mathematical Modelling 36 (1) (2012) 379–398. doi:10.1016/j.apm.2011.07.032.

[20] P. R. Spalart, Philosophies and fallacies in turbulence modeling, Progress in Aerospace Sciences 74 (2015) 1–15. doi:10.1016/j.paerosci.2014.12.004.

[21] A. Elmiligui, K. Abdol-Hamid, S. Massey, S. Pao, Numerical study of flow past a circular cylinder using hybrid turbulence formulations, . Journal of Aircraft 47 (2) (2010) 434–440.

[22] J. Tyacke, R. Jefferson-Loveday, P. G. Tucker, On the application of les to seal geometries, Flow, Turbulence and Combustion 91 (4) (2013) 827–848. doi:10.1007/s10494-013-9480-x.

[23] J. Holgate, A. Skillen, T. Craft, A. Revell, A review of embedded large eddy simulation for internal flows, Archives of Computational Methods in Engineering 26 (4) (2018) 865–882. doi:10.1007/s11831-018-9272-5.

[24] F. Roknaldin, A. Panigrahy, Board level thermal analysis via large eddy simulation (les) tool, The Ninth Intersociety Conference on Thermal and Thermomechanical Phenomena In Electronic Systems (IEEE Cat. No.04CH37543) (2004). doi:10.1109/itherm.2004.1319218.

[25] P. Weihing, B. Younis, B. Weigand, Heat transfer enhancement in a ribbed channel: Development of turbulence closures, International

Journal of Heat and Mass Transfer 76 (2014) 509–522. doi:10.1016/j.ijheatmasstransfer.2014.04.052.

[26] H. Iacovides, M. Raisee, Recent progress in the computation of flow and heat transfer in internal cooling passages of turbine blades, International Journal of Heat and Fluid Flow 20 (3) (1999) 320–328. doi:10.1016/s0142-727x(99)00018-1.

[27] B. K. Lodh, A. K. Das, N. Singh, Numerical comparison of rans and les turbulence model for wind flow over a cube in a turbulent channel using openfoam, International Journal of Engineering Research and V6 (02) (2017). doi:10.17577/ijertv6is020303.

[28] A. Dastbelaraki, M. Yaghoubi, M. M. Tavakol, A. Rahmatmand, Numerical analysis of convection heat transfer from an array of perforated fins using the reynolds averaged navier–stokes equations and large-eddy simulation method, Applied Mathematical Modelling 63 (2018) 660–687. doi:10.1016/j.apm.2018.06.005.

[29] P. Spalart, Strategies for turbulence modelling and simulations, International Journal of Heat and Fluid Flow 21 (3) (2000) 252–263. doi:10.1016/s0142-727x(00)00007-2.

[30] S. B. Pope, Turbulent flows, Cambridge University Press, 2000.

[31] Y. Liu, P. Tucker, R. Kerr, Linear and nonlinear model large-eddy simulations of plane jet, 44th AIAA Aerospace Sciences Meeting and Exhibit (2006). doi:10.2514/6.2006-702.

[32] J. Tyacke, Low reynolds number heat transfer prediction employing large eddy simulation for electronics geometries, Ph.D. thesis, Swansea University (2009).

[33] P. A. Durbin, Some recent developments in turbulence closure modeling, Annual Review of Fluid Mechanics 50 (1) (2018) 77–103. doi:10.1146/annurev-fluid-122316-045020.

[34] A. Afzal, Z. Ansari, A. R. Faizabadi, M. K. Ramis, Parallelization strategies for computational fluid dynamics software: State of the art review, Archives of Computational Methods in Engineering 24 (2) (2016) 337–363. doi:10.1007/s11831-016-9165-4.

[35] H. K. Versteeg, W. Malalasekera, An introduction to computational fluid dynamics: the finite volume method, Pearson/Prentice Hall, 2010.

[36] A. Hellsten, P. Rautaheimo, S. Laine, T. Siikonen, Proceedings of ERCOFTAC/IAHR/COST Workshop on Refined Turbulence Modelling (8th), 1999.

[37] B. Launder, B. Sharma, Application of the energy-dissipation model of turbulence to the calculation of flow near a spinning disc, Letters in Heat and Mass Transfer 1 (2) (1974) 131–137. doi:10.1016/0094-4548(74)90150-7.

[38] C. R. Yap, Turbulent heat and momentum transfer in recirculating and impinging flows, Ph.D. thesis, University of Manchester (1987).

[39] A. Yoshizawa, Bridging between eddy-viscosity-type and second-order turbulence models through a two-scale turbulence theory, Physical Review E 48 (1) (1993) 273–281. doi:10.1103/physreve.48.273.

[40] E. Meinders, K. Hanjalić, Vortex structure and heat transfer in turbulent flow over a wall-mounted matrix of cubes, International Journal of Heat and Fluid Flow 20 (3) (1999) 255–267. doi:10.1016/s0142-727x(99)00016-8.

[41] E. R. Meinders, Experimental study of heat transfer in turbulent flows over wall-mounted cubes, Ph.D. thesis, Delft University of Technology (1998).

[42] W. George, Lectures in turbulence for the 21st century (2013).